Dimethyl Ether Oxidation at Elevated Temperatures (295−600 K)

Claudette M. Rosado-Reyes and Joseph S. Francisco*

Department of Chemistry and Department of Earth and Atmospheric Sciences, Purdue University, West Lafayette, Indiana 47907

Joseph J. Szente and M. Matti Maricq

Physical & Environmental Sciences Department, Research and Advanced Engineering, Ford Motor Company, P.O. Box 2053, Drop 3083, Dearborn, Michigan 48121

Lars Frøsig Østergaard

Department of Radiation Research, Risø National Laboratory, Frederiksborgvej 399, P.O. Box 49, DK-4000 Roskilde, Denmark

Received: July 29, 2005; In Final Form: October 4, 2005

Dimethyl ether (DME) has been proposed for use as an alternative fuel or additive in diesel engines and as a potential fuel in solid oxide fuel cells. The oxidation chemistry of DME is a key element in understanding its role in these applications. The reaction between methoxymethyl radicals and O_2 has been examined over the temperature range 295−600 K and at pressures of 20−200 Torr. This reaction has two product pathways. The first produces methoxymethyl peroxy radicals, while the second produces OH radicals and formaldehyde molecules. Real-time kinetic measurements are made by transient infrared spectroscopy to monitor the yield of three main products—formaldehyde, methyl formate, and formic acid—to determine the branching ratio for the $CH_3OCH_2 + O_2$ reaction pathways. The temperature and pressure dependence of this reaction is described by a Lindemann and Arrhenius mechanism. The branching ratio is described by $f = 1/(1 + A_T[M])$, where $A_T = (1.6^{+2.4}_{-1.0} \times 10^{-20}) \exp((1800 \pm 400)/T)$ cm^3 molecule^{-1}. The temperature dependent rate constant of the methoxymethyl peroxy radical self-reaction is calculated from the kinetics of the formaldehyde and methyl formate product yields, $k_4 = (3.0 \pm 2.1) \times 10^{-13} \exp((700 \pm 250)/T)$ cm^3 molecule^{-1} s^{-1}. The experimental and kinetics modeling results support a strong preference for the thermal decomposition of alkoxy radicals versus their reaction with O_2 under our laboratory conditions. These characteristics of DME oxidation with respect to temperature and pressure might provide insight into optimizing solid oxide fuel cell operating conditions with DME in the presence of O_2 to maximize power outputs.

Introduction

The fact that current diesel engine emissions will not meet future standards has spurred research into alternative fuels in order to reduce emissions without compromising fuel economy. Oxygenated hydrocarbons such as ethers have been proposed for use as alternative fuels or as additives in diesel engines.[1] The chemical and thermodynamic properties of dimethyl ether (DME) make it ideal for this purpose:[2−5] higher cetane number of 55−60, lower self-ignition temperatures, reduced NO_x emissions and engine noise, and no soot formation. Having an atmospheric lifetime of approximately 8 days,[6] DME shows a low tropospheric ozone-forming potential and degrades easily in the atmosphere. Determining the emissions produced from the use of DME as a diesel fuel is required to assess its impact on atmospheric reactivity models.

DME has also been under consideration as a fuel for solid oxide fuel cells (SOFCs)[7,8] and polymer electrolyte membrane (PEM) fuel cells.[9] SOFCs offer a clean, pollution-free technology to electrochemically generate electricity at high efficiencies.[10] For vehicle-based fuel cells, the direct oxidation of hydrocarbons at temperatures above 500 °C eliminates the need for an external fuel reformer system and can reduce the cost and weight of SOFC systems. The temperature dependence of DME thermal decomposition is important in determining the power output of SOFCs and their contamination by coking. The feasibility of operating SOFCs at low to medium temperatures has been explored by introducing DME directly into the cell.[7] DME fuel operated SOFCs achieved reasonable power densities and avoided carbon deposition for temperatures below 750 °C. Improved power densities were obtained at temperatures between 550 and 650 °C when mixtures of DME + air were used in place of pure DME.[8] Lower operating temperatures ensure greater overall system efficiency and a reduction of thermal stress in the active ceramic structure.

The physical properties of DME are similar to those of liquid petroleum gas (propane and butane).[11] At room temperature, DME is a liquid at 0.6 MPa (75 psig). Therefore, the existing liquid propane infrastructure can be used to handle, transport, and store DME. The manufacture of DME on a small commercial scale is currently achieved by fixed bed catalytic dehydration of methanol.[12] Although this process is relatively expensive, it produces DME of very high purity. An alternative

10.1021/jp054223t CCC: $30.25 © 2005 American Chemical Society
Published on Web 11/12/2005

way of producing DME on a larger scale but at lower cost has been developed on the basis of the autothermal reforming of natural gas.

Atmospheric degradation of dimethyl ether (CH_3OCH_3) is initiated via hydrogen abstraction by OH radicals. Under laboratory conditions, chlorine atoms—produced by the photolysis of Cl_2—initiate the chemistry. Methoxymethyl radicals (CH_3OCH_2) are produced as a result of the abstraction of a methyl hydrogen from DME. Under high O_2 concentrations, methoxymethyl radicals combine with oxygen to produce methoxymethyl peroxy radicals ($CH_3OCH_2O_2$). Previous product studies of chlorine-initiated chemistry at room temperature showed a dependence on total pressure, where production of formaldehyde and production of methyl formate compete against each other.[6,13] This pressure dependence was explained by proposing and showing that the oxidation of dimethyl ether proceeds via two different competitive pathways: a pressure dependent pathway and a pressure independent one

$$Cl_2 + 351\ nm \rightarrow 2Cl \quad (1)$$

$$CH_3OCH_3 + Cl \rightarrow CH_3OCH_2 + HCl \quad (2)$$

$$CH_3OCH_2 + O_2 \rightarrow CH_3OCH_2O_2^* + M \rightarrow CH_3OCH_2O_2 + M \quad (3a)$$

$$CH_3OCH_2 + O_2 \rightarrow CH_3OCH_2O_2^* \rightarrow CH_2OCH_2O_2H \rightarrow 2HC(O)H + OH \quad (3b)$$

$$2CH_3OCH_2O_2 \rightarrow 2CH_3OCH_2O + O_2 \quad (4a)$$

$$2CH_3OCH_2O_2 \rightarrow CH_3OC(O)H + CH_3OCH_2OH + O_2 \quad (4b)$$

In the pressure dependent pathway (reaction 3a), the energetically excited peroxy (RO_2^*) is collisionally deactivated into a stabilized peroxy radical that can continue reacting by usual peroxy radical reactions (reactions 4a and 4b). From these methoxymethyl peroxy radical reactions, methyl formate ($CH_3OC(O)H$) and methoxy methylhydroperoxy (CH_3OCH_2OH) are formed as the main products. The pressure independent pathway (reaction 3b) takes place via the intramolecular rearrangement of the peroxy radical followed by dissociation into two molecules of formaldehyde and one hydroxyl radical. This pressure independent pathway is of particular interest with respect to combustion because OH radicals are an important reactive intermediate in combustion processes. The production of hydroxyl radicals can initiate and sustain a chain reaction between DME and OH.

The kinetics and degradation of DME have been previously studied under atmospheric conditions.[14−17] Japar et al. (1990) studied the mechanism for the Cl-initiated and OH-initiated atmospheric oxidation of some proposed oxygenated fuel additives, including dimethyl ether, by Fourier transform IR (FTIR) spectroscopy at 295 K and 700 Torr. Only methyl formate was observed as the major product, having a yield of 0.90 ± 0.08 relative to DME loss. Jenkin et al. (1993) measured the UV absorption spectrum of the methoxymethyl peroxy radical in the range 200−290 nm and the kinetics of the $CH_3OCH_2O_2$ self-reaction. The second-order kinetics of methoxymethyl peroxy radicals showed the reaction to be sensitive to the total pressure between 70 and 760 Torr and to the composition of the reaction mixture. In addition, their results supported rapid thermal decomposition of methoxymethyl alkoxy radicals (CH_3OCH_2O) by ejecting H atoms (reaction 5), which occurs in competition with the reaction with O_2 (reaction 6) to form HO_2 radicals and methyl formate.

$$CH_3OCH_2O \rightarrow CH_3OC(O)H + H \quad (5)$$

$$CH_3OCH_2O + O_2 \rightarrow CH_3OC(O)H + HO_2 \quad (6)$$

Langer et al. (1995) studied the gas-phase chemistry of methoxymethyl and methoxymethyl peroxy radicals at 296 K and a total pressure of 1000 mbar. Pulse radiolysis−UV absorption was utilized to measure the UV spectrum of methoxymethyl radicals and to quantify the rate constants for the reaction of methoxymethyl peroxy with NO and NO_2. Sehested et al. (1996) focused their experimental work on the kinetics and mechanism involved in the reaction of $CH_3OCH_2 + O_2$ at 296 K and 0.38−940 Torr total pressure using the FTIR smog chamber technique. The effect of pressure on the reaction was observed between 2 and 200 Torr. At the low-pressure limit, formaldehyde reached a yield of ~200% at 0.38 Torr. The high-pressure limit product distribution showed a combined yield of methyl formate ($CH_3OC(O)H$) and methoxy methylhydroperoxy (CH_3OCH_2OH) of 100% at 700 Torr. Maricq et al. (1997) measured the reaction between methoxymethyl radicals and molecular oxygen using transient IR absorption to monitor formaldehyde formation at 230−350 K and 5−80 Torr total pressure. The branching ratio for reactions 3a and 3b was described using a modified Lindemann mechanism. On the basis of the formaldehyde yields, it was observed that, as the temperature is increased, the reaction shifts to enhanced formaldehyde production, but this change is not as significant as the pressure dependence. These results raised the possibility that, at even higher temperatures, the methoxymethyl peroxy radical dissociation channel might become significant enough to sustain the DME + OH chain reaction which could be important for low-temperature combustion. However, the results were limited by the narrow temperature range and the measurement of formaldehyde formation only. Sehested et al. (1997) studied the reaction of methoxymethyl radicals with molecular oxygen in the temperature range 296−473 K and at a high pressure of 18 bar by pulse radiolysis coupled with time-resolved UV absorption spectroscopy. The high-pressure limit rate constant for the addition of oxygen to CH_3OCH_2 was determined to be $(1.07 \pm 0.08) \times 10^{-11} \exp(-(46 \pm 27)/T)$ cm^3 molecule^{-1} s^{-1}.

Andersen and Carter[18,19] used hybrid density functional theory (DFT) methods to study the potential energy surface of the chain propagation step in low-temperature dimethyl ether oxidation, which involves the decomposition of CH_2OCH_2OOH into two HC(O)H molecules and one OH radical. The extent to which $HO_2CH_2OC(O)H$ (hydroperoxy methyl formate), produced from the chain branching step (addition of O_2 to CH_2OCH_2OOH), could sustain a chain reaction was also explored. The examination of the energetics of six competitive pathways showed that the decomposition of hydroperoxy methyl formate could take place via the following two most favorable mechanisms: the O−O bond scission and the Criegee intermediate ($\cdot CH_2OO\cdot$) and formic acid pathways, both requiring an activation energy of 42 kcal/mol.

Several studies have examined the oxidation chemistry and pyrolysis of DME in the combustion regime.[20−25] Pfahl et al. (1996) investigated the gas-phase self-ignition behavior of diesel-relevant hydrocarbon/air mixtures on the basis of their measured ignition delay times in a shock tube, for temperatures of 650−1300 K and high pressures (13 and 40 bar, $\phi = 1$) occurring in diesel engines. Dagaut et al. (1996) reported the first experimental kinetic study on dimethyl ether oxidation at

high temperatures (800−1300 K) in a fused silica jet-stirred reactor over 1−10 atm and $0.2 \leq \phi \leq 2.0$, and in a later study, Dagaut et al. (1998) extended their measurements to lower temperatures (550−1100 K). From both studies, it was concluded that DME exhibits typical "two-stage" ignition characteristics common to many hydrocarbons. Curran et al. (1998) developed a kinetic model to simulate the jet-stirred reactor and shock-tube experimental results over a broad temperature range, 650−1300 K, where both low- and high-temperature chemistry contribute to fuel oxidation. The model was able to accurately predict concentration profiles for each product species and total ignition delay times. Fisher et al. (2000) conducted DME pyrolysis studies in a variable-pressure flow reactor at 2.5 atm, 1060 K, and 99.7% nitrogen dilution. Oxidation experiments were also performed in an atmospheric-pressure flow reactor at 1086 K, a nitrogen dilution of 98%, and $0.32 \leq \phi \leq 3.4$. The developed kinetic model, consisting of 351 elementary reactions and 82 chemical species, reproduced fuel and intermediate byproduct profiles with a high degree of accuracy. Curran, Fisher, and Dryer (2000), with the purpose of improving the understanding of the low- and intermediate-temperature DME oxidation (550−850 K), obtained new results from a variable-pressure flow reactor in the pressure range 12−18 atm, at a 98.5% nitrogen dilution, and at $0.7 \leq \phi \leq 4.2$, by the FTIR technique. The data revealed formic acid as a major intermediate product. The previously modified kinetics modeling incorporated a pathway involving the rearrangement and further decomposition of the $OCH_2OC(O)H$ radical into formic acid and hydrogen atoms.

Liu and co-workers[26] have conducted other atmospheric-pressure laminar flow reactor experimental studies. The influence of nitric oxide on DME oxidation was investigated at a temperature range from 240 to 700 °C over 2−4 s residence times. Reaction products were monitored by Fourier transform IR spectroscopy, from the decomposition of 340 ppm DME in 10% oxygen. CO, formaldehyde, and formic acid were observed as major byproducts. The addition of NO resulted in the production of methyl formate between 300 and 400 °C. Also, CO_2 and formic acid were observed in significant concentrations below 500 °C. These results were shown to be qualitatively consistent with the ones reported by Dagaut et al. (1998).

Most of the previous work on DME oxidation has been performed under either conditions approximating atmospheric temperatures and pressures or in the combustion regime. The oxidation chemistry of DME at relatively low temperatures of 295−600 K may provide some useful information about its behavior at the elevated temperatures. The present study was undertaken to determine the branching ratio for the $CH_3OCH_2 + O_2$ reaction pathways at pressures of 20−200 Torr and the importance of dimethyl ether degradation in the presence of O_2 over the low- and intermediate-temperature range 295−700 K.

Experimental Section

To investigate the temperature dependence on the degradation of dimethyl ether and consequently on the $CH_3OCH_2 + O_2$ branching ratio, the kinetics of the reaction of $CH_3OCH_3 + Cl_2$ in the presence of O_2 is being studied at elevated temperatures. Flash photolysis/transient infrared spectroscopy is used to evaluate the yield and kinetics of formaldehyde, methyl formate, and formic acid as they are produced during DME oxidation chemistry. The measurements include direct probing of IR absorbances of these products in the carbonyl stretching region 1700−1800 cm^{-1}. These experiments are carried out over the temperature range 295−600 K at three different total concentration densities of 65, 250, and 650×10^{16} molecules/cm^3, which will also be referred to as the low-, medium-, and high-pressure conditions. These concentrations correspond to room-temperature pressures of 20, 75, and 200 Torr, respectively. To maintain consistency in the individual and total gas densities over this temperature range, concentrations are held constant at the various temperatures, not pressures.

The flash photolysis/time-resolved IR spectroscopy experimental apparatus is described as follows (Figure 1). A reagent gas mixture is inserted into a quartz cylindrical reaction cell. The beam from an IR tunable diode laser propagates along the axis of the cell to monitor the DME oxidation products. A pulsed UV excimer laser beam counterpropagates through the reaction cell to initiate the chemistry via Cl_2 photolysis. The details of this system are given below.

The gas mixtures for these experiments consisted of dimethyl ether (1−7 Torr), 4.8% chlorine/N_2 (2−11 Torr), O_2 (11−38 Torr), and N_2 to make up the balance. Gas flows are adjusted with Tylan/Millipore mass flow controllers. Individual gas flow rates are determined by measuring the rate of pressure change while flowing a selected gas into a fixed volume. The partial pressure for each gas in the mixture is its fraction of the total flow rate multiplied by the total pressure. Reference gas mixtures of formaldehyde, methyl formate, and formic acid are used to measure IR absorbance cross sections. These reference mixtures are prepared by diluting a specific amount of a selected gas with nitrogen in a 5 L Pyrex flask. Photodissociation of Cl_2 into chlorine atoms is initiated by firing 351 nm laser light into the gas mixture from a Lambda Physik model LPX-301 excimer laser, operating at a repetition rate of 0.5 s and 300−600 mJ per pulse. Initial Cl radical concentrations are between 5 and 15×10^{14} molecules/cm^3 depending on the Cl_2 concentration and laser energy. Dichroic beam-steering mirrors located at opposite ends of the flow cell direct the excimer laser beam along the axis of the cell and then out of the optical path to a "beam dump". The conditions are such that the gas mixture is replenished between laser pulses.

The cylindrical quartz reaction cell is wrapped with electrical heaters and insulated to attain desired temperatures. A stable temperature within the reaction cell is achieved by separating the cell into different sections, as illustrated in Figure 2. Reactants are preheated in the U-shaped inlet tube prior to entering the center section of the cell. This reactive region is 3.3 cm in diameter and 48 cm in length. The outer "buffer" sections are 3.7 cm in diameter and 11 cm in length and are filled with a steady flow of nitrogen to prevent the reactant mixture from leaking into these sections. BaF_2 windows are used to close the ends of the flow cell. The center and outer sections are separated by BaF_2 windows that are held in place by stainless steel springs positioned between the inner and outer windows. These outer sections minimize temperature gradients within the reaction mixture. At the ends of the cell, the temperature can change by as much as 50 °C/cm for the first 5 cm, but it stabilizes within 10 cm of the ends and inner temperatures are ±10 °C of the measured temperature over the active region of the cell. Temperature is monitored and controlled by an Omega heater controller (CN3910A) in combination with thermocouples positioned along the outside of the cell. BaF_2 is used for the cell windows and the excimer laser dichroic mirrors because it allows the transmission of the UV laser light as well as the IR light from the diode laser and resists rapid degradation at the higher temperatures. The interior windows are wedges with one surface at an angle of 0.25° from parallel. The outer windows are plane parallel windows mounted at a 2° angle with respect

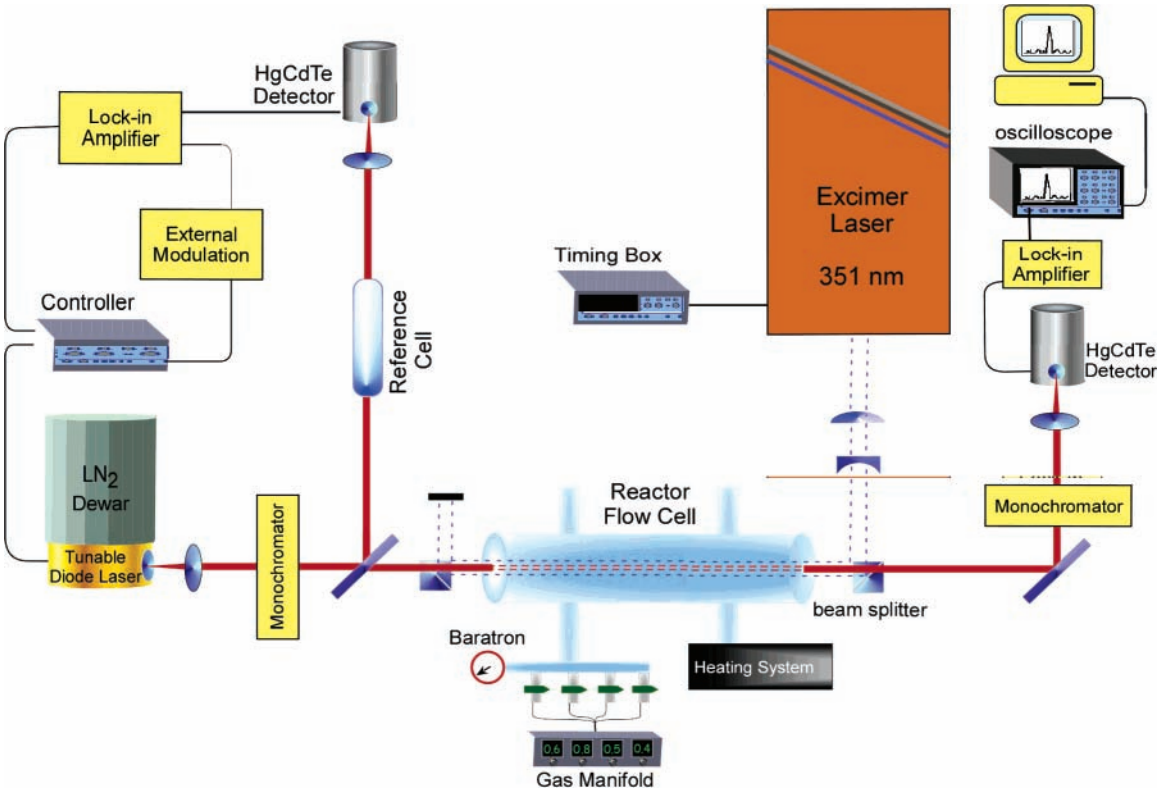

Figure 1. Flash photolysis/time-resolved IR spectroscopy experimental apparatus.

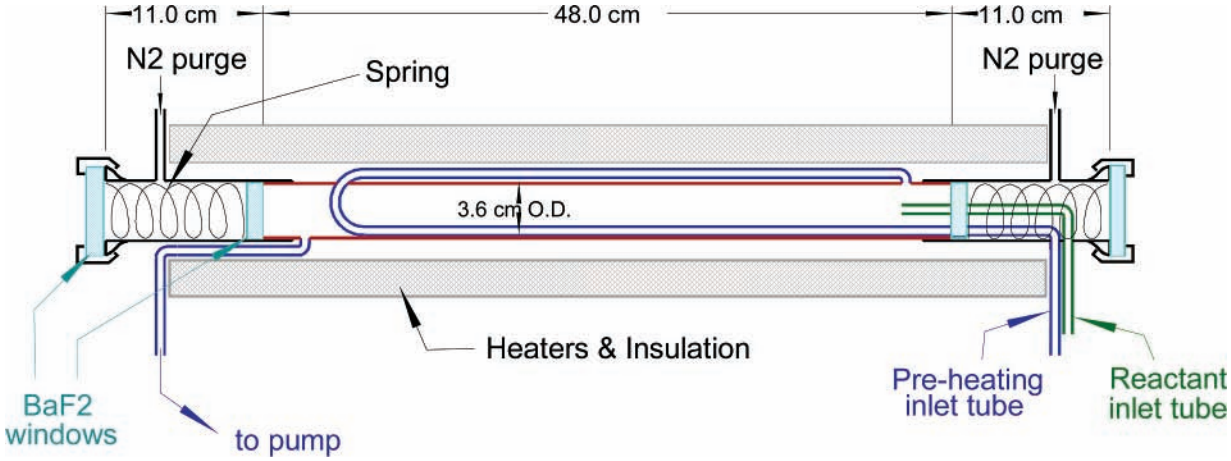

Figure 2. Schematic diagram of the heated quartz reactor cell.

to the vertical. The arrangement of both inner and outer windows prevents back reflections of the excimer laser beam from reaching the IR detector.

A high-resolution, cryogenically cooled (77 K) Pb-salt tunable diode laser (TDL) is used as the infrared light source to probe the rovibrational carbonyl stretch mode of the products at frequencies between 1700 and 1800 cm^{-1}. The tunable diode laser system (Laser Components IG, Inc.) consists of a laser source dewar (model L5736), a microprocessor-controlled temperature and current controller for precise tuning (model L5830), a confocal Etalon, and an optical system designed to collimate, direct, and detect the output from the TDL. The selection of IR absorbance lines (1709, 1742, and 1791 cm^{-1}) is based on the respective absorbance bands of the three species of interest. Figure 3 shows FTIR absorbance spectra for formaldehyde, methyl formate, and formic acid along with the selected frequencies. The P, Q, and R branches are clearly shown. At 1709 cm^{-1}, formaldehyde has strong absorbance lines but methyl formate and formic acid are much weaker. For the other two probe frequencies, 1742 cm^{-1} is chosen for strong methyl formate absorption and 1791 cm^{-1} is chosen for strong formic acid absorption. In addition, methyl formate presented a complication to the measurements because of its broad, mostly unstructured spectrum. In most cases, the high resolution of the TDL makes it possible to select the frequency of an isolated absorbance line of a particular species, even if another species has an overlapping spectrum. The separation between line peaks makes it possible to monitor one species while excluding the other. When pressure broadening has caused the line widths to expand to the point where they overlap each other, then it becomes necessary to consider the contribution to the absorbance from both species. Since the methyl formate absorbance lines are completely overlapped, even at a pressure of 1 Torr, it interferes with measurement of absorbance peaks for any frequency within the region of the methyl formate absorbance bands. Absorbance measurements are made both at the peak of

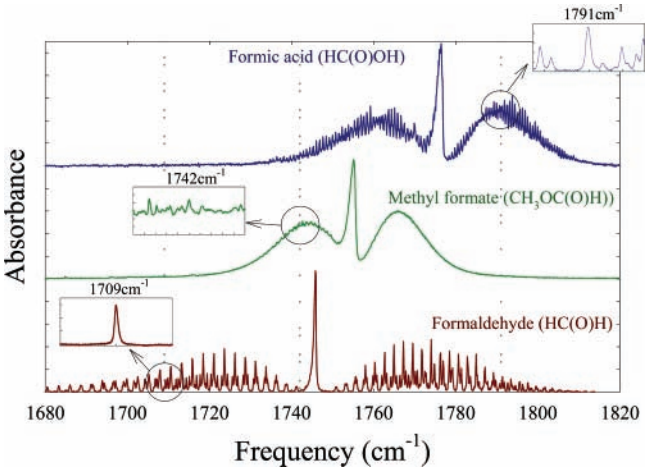

Figure 3. FTIR spectra of formaldehyde, methyl formate, and formic acid (provided by Mike Hurley, Ford Research Laboratory).

the absorbance line (on-line) and at the nearest minimum adjacent to the absorbance line (off-line). This enables the absorbance due to the species of interest to be separated from the contribution of methyl formate.

For the kinetic measurements, the diode laser is frequency locked to the peak of an absorbance line in the following manner. The diode laser is first tuned to the center of an absorption line. An external modulation of 5.6 kHz is applied to the diode laser current. This modulation is small compared to the line width. The IR beam is split into two portions, one directed to the reaction cell and the other directed to a reference gas cell (typically 5−10 cm in length). The portion of the IR beam directed through the reference gas cell is detected by a HgCdTe detector. A lock-in amplifier uses the signal from the reference cell detector to keep the TDL fixed at the peak of the absorbance line being monitored and prevent frequency drift. The main IR beam is directed along the axis of the flow cell, in the opposite direction of the excimer laser beam. Dichroic beam-steering mirrors on BaF_2 substrates located outside of the flow cell direct the excimer laser beam through the cell and allow the IR laser beam to travel within the volume traced by the photolysis beam. The IR light is then focused by a second monochromator (model HR640, Instruments SA, Inc.) with a 75 line/mm, 10 μm blaze grating to prevent extraneous light from reaching the LN_2 cooled HgCdTe detector. The IR detector has a response time of 0.3 μs, and its output is amplified and recorded by a Tektronix digital oscilloscope (model TDS 460A).

Since the detector responds to changes in IR light intensity, the sampled signal (ΔI_t) represents the change in light intensity in the absence and presence of a light absorber. Absolute beam intensity is measured by amplitude modulating the diode laser radiation at 2 kHz with a mechanical chopper and recording the detector response as it oscillates from no light to full light exposure. The initial light intensity (I_0) is the amplitude of the IR beam reaching the detector with all of the optical components in place, but without the gas mixture flowing. The intensity before the laser is fired (I_b) is measured with the gas mixture flowing through the cell. The absorbance is then calculated by adding the transient light intensity change to the light intensity before laser photolysis and comparing it to the reference tunable diode laser light intensity as

$$\text{absorbance}(t) = \ln\left(\frac{-(I_b + \Delta I_t)}{I_0}\right) \tag{7}$$

When on-line and off-line measurements are taken, the off-line absorbance is subtracted from the on-line absorbance to obtain the absolute absorbance contribution for a particular absorber. IR absorption cross sections (σ) are determined by flowing a known concentration of the reference gas into the reactor cell at the particular pressure and temperature and measuring the absorbance at the selected IR frequency. Transient concentrations over the 900 μs sampling time after photolysis are calculated from Beer's law

$$C(t) = \left(\frac{1}{l\sigma}\right) \ln\left(\frac{-(I_b + \Delta I_t)}{I_0}\right) \tag{8}$$

The initial halogen radical concentration from photolysis is calculated indirectly by substituting methanol for DME and measuring the formaldehyde yield. A 100% conversion is obtained from methanol to formaldehyde. Chlorine-initiated methanol oxidation takes place as follows

$$CH_3OH + Cl \rightarrow CH_2OH + HCl \tag{9}$$

$$CH_2OH + O_2 \rightarrow HC(O)H + HO_2 \tag{10}$$

The measured HC(O)H yield is used to calculate the concentration of initial Cl atoms.

DME thermal oxidation at temperatures above 450 K made it necessary to determine the concentration of formaldehyde, methyl formate, and formic acid in the gas mixture prior to Cl_2 photolysis. Mixtures of DME, O_2, and N_2 are probed with the IR beam while flowing through the reactor cell at total concentrations of 65, 250, and 650 $\times$ 10^{16} molecules/cm^3 and at temperatures between 295 and 700 K, in 50 K increments. The gas flow rates are selected such that the residence time in the cell is between 2 and 4 s at the various pressures and temperatures. The experimental apparatus is the same; however, the technique for measuring IR absorbances was modified. DME thermal oxidation measurements are performed by scanning across a 0.4 cm^{-1} band of the IR spectrum centered around a selected absorbance line. The absorbance is obtained by ramping the TDL current over a selected set of spectral lines at a rate of 2.5 Hz while amplitude modulating the diode laser beam at 2.0 kHz with a mechanical chopper. The signal from the reaction cell IR detector is fed into a lock-in amplifier (model SR850, Princeton Instruments). The DC output from the lock-in amplifier, which is proportional to the absolute intensity of the IR signal after absorption from the respective byproducts, is averaged and recorded into a digital scope. A confocal Etalon is utilized to calibrate the width of the diode current ramp in wavenumbers. In addition to these measurements, at each temperature and pressure condition, the DME is replaced with a known concentration of each of the reference gases (HC(O)H, $CH_3OC(O)H$, and HC(O)OH) and the scan is repeated to obtain the corresponding IR cross-sectional spectra. The IR frequency scans provide more information about the products at each frequency region of 1709, 1742, and 1791 cm^{-1}, but due to the added signal processing with the lock-in amplifier, they required approximately 0.5 s to complete each measurement. This method is suitable for monitoring the steady state concentrations of the products but would not be appropriate for the kinetics measurements which require a data acquisition rate around 2 MHz. The absorbance is calculated using $\ln[-I/I_0]$, where I_0 is the full scale IR signal intensity with an O_2/N_2 mixture and I is the IR signal intensity when the reference gas is flowing along with O_2/N_2. Measured IR absorption spectra from DME/O_2/N_2 reaction mixtures may consist of the superposition of one or more IR absorbance bands from formaldehyde, methyl formate,

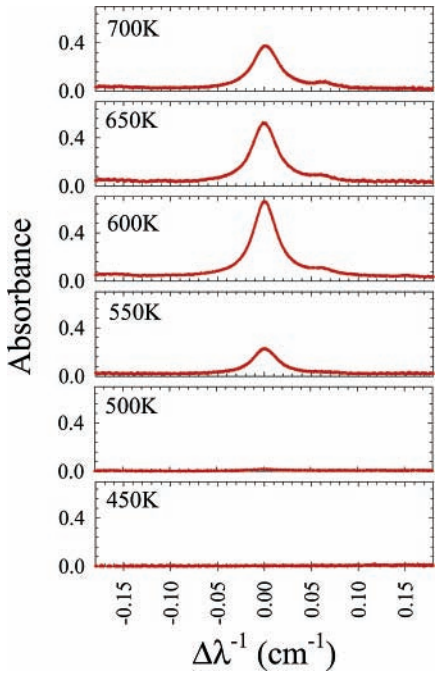

Figure 4. TDL frequency scan at 1709 cm^{-1} for the temperature range 450−700 K. Formaldehyde production from DME oxidation. [DME] = 13 × 10^{16}/cm^3, [O_2] = 56 × 10^{16}/cm^3, and P_{tot} = 250 × 10^{16}/cm^3.

and formic acid. The individual contribution of each byproduct to the total absorbance is determined through Beer's law by deconvolving the overall absorption spectrum into the respective individual concentrations, as

$$A_{\text{total}} = \sum \sigma_i C_i l \tag{11}$$

where A_{total} is the total measured absorbance, σ_i is the calculated individual IR cross sections, l is the path length, and C_i is the individual concentrations from the deconvolution fit.

Results

A. Thermal Oxidation of Dimethyl Ether. In the flash photolysis method, the chemistry is initiated at $t = 0$ by a laser pulse and the kinetics deduced by following in time the subsequent formation and disappearance of radicals such as CH_3OCH_2 and $CH_3OCH_2O_2$. However, in the presence of oxygen and at temperatures above 500 K, DME undergoes spontaneous degradation. This causes the removal of DME and the formation of radical intermediates that interfere with the analysis of the photolysis data. Therefore, a separate set of measurements was undertaken to investigate the thermal decomposition mechanism of DME in the presence of oxygen. In these experiments, a gas mixture of DME/O_2/N_2 is allowed to equilibrate to a selected temperature while flowing through the reactor cell. Figure 4 shows the absorbance measurements recorded by frequency scans over the IR absorbance line at 1709 cm^{-1}. There is a clear temperature effect on the formaldehyde absorbance. A measurable absorbance is detected at 500 K, reaches a maximum at 600 K, and decreases above that temperature.

Figure 5 shows the product yields from DME thermally induced oxidation, in the absence of chlorine, normalized to the initial dimethyl ether concentrations at temperatures between 295 and 700 K, in increments of 50 K. As with formaldehyde, the concentrations of formic acid and methyl formate increase with temperature, reaching maximum levels between 600 and 650 K, and then decline. At low pressure, the formaldehyde yield is smaller than that at medium and high pressure, but the

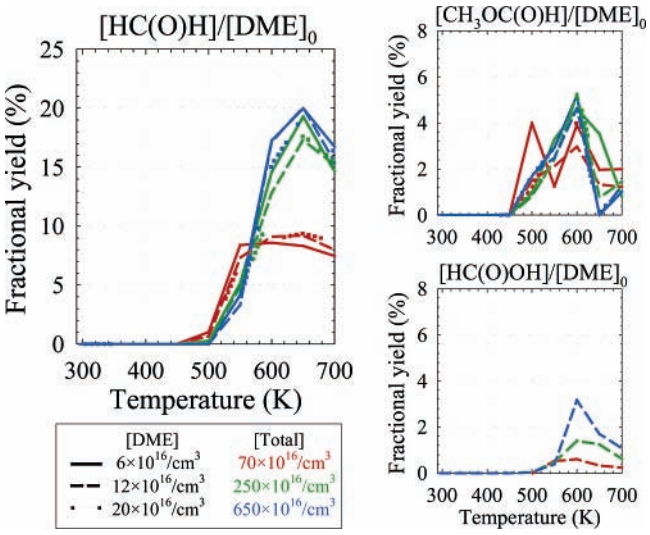

Figure 5. Formaldehyde, methyl formate, and formic acid yields relative to dimethyl ether initial concentration in the temperature regime 295−700 K at three different total pressure conditions.

change between medium and high pressure is not significant. The methyl formate and formic acid yields follow a similar trend, although the formaldehyde yield is greater by a factor of 4 and 7, respectively.

Figure 5 also shows that the relative formaldehyde yield is independent of DME initial concentration. The formaldehyde yield reaches a maximum of 20% of the initial DME concentration for the high-pressure case. Formaldehyde formation appears to have reached a high-pressure limit by a total number density of 250 × 10^{16} molecules/cm^3. The formic acid yield also increases with pressure, reaching 3% of the initial DME concentration. On the other hand, methyl formate shows no discernible pressure dependence and reaches a maximum of 5% of the initial DME concentration. Even though our operating conditions are much lower in pressure than many of the prior studies performed in this temperature regime,[18,20−22] the product yields follow a similar trend: emergence of products at temperatures between 450 and 530 K, maximum yield of products around 575−650 K, and a sudden decrease of product yields above 650 K. This trend is characteristic of the observed DME two-stage ignition behavior, as described by Pfahl et al.[20] and Dagaut et al.[22]

The data show a significant fraction (at least 10−20%) of DME decomposing at temperatures above 600 K, based on the formaldehyde yield. Under these conditions, production of the alkyl radical proceeds via one of the following hydrogen abstraction reactions

$$CH_3OCH_3 + O_2 \rightarrow CH_3OCH_2 + HO_2 \tag{12}$$

$$CH_3OCH_3 + OH \rightarrow CH_3OCH_2 + H_2O \tag{13}$$

$$CH_3OCH_3 + H \rightarrow CH_3OCH_2 + H_2 \tag{14}$$

which then undergoes oxygen addition (reactions 3a and 3b). The decomposition of DME not only produces formaldehyde, methyl formate, and formic acid but also produces many other species from secondary reactions (e.g., H, OH, HO_2, and CH_3). These intermediate species react with DME, and with the other secondary products. This complicates the interpretation of kinetics measurements above 600 K. Furthermore, the loss of available IR light, due to the high concentrations of these secondary products, interferes with the ability to quantify their

TABLE 1: Mechanism for the $CH_3OCH_2 + O_2$ Reaction

	reaction[a]	k (cm^3 $molecule^{-1}$ s^{-1})	ref
	Initiation Reactions		
2	$CH_3OCH_3 + Cl \rightarrow CH_3OCH_2 + HCl$	1.9×10^{-10}	15
12	$CH_3OCH_3 + O_2 \rightarrow CH_3OCH_2 + HO_2$	$6.8 \times 10^{-11} \exp(-22\,600/T)$	24
13	$CH_3OCH_3 + OH \rightarrow CH_3OCH_2 + H_2O$	$1.0 \times 10^{-11} \exp(-370/T)$	30
14	$CH_3OCH_3 + H \rightarrow CH_3OCH_2 + H_2$	$4.4 \times 10^{-12} \exp(-1960/T)$	31
	$CH_3OCH_3 \rightarrow CH_3O + CH_3$	$3.2 \times 10^{16} \exp(-41\,800/T)$ s^{-1}	32
	Alkyl Radical Reactions		
3a	$CH_3OCH_2 + O_2 + M \rightarrow CH_3OCH_2O_2 + M$	$(1 - f)(3.1 \times 10^{-12} \exp(326/T))$	13, this work
3b	$CH_3OCH_2 + O_2 \rightarrow 2HC(O)H + OH$	$f(3.1 \times 10^{-12} \exp(326/T))$	13, this work
	$CH_3OCH_2 + Cl_2 \rightarrow CH_3OCH_2Cl + Cl$	$1.8 \times 10^{-11} \exp(360/T)$	13
	$CH_3OCH_2 + Cl \rightarrow CH_3OCH_2Cl$	$(0-2) \times 10^{-10}$	13
	Peroxy Radical Reactions		
4a	$CH_3OCH_2O_2 + CH_3OCH_2O_2 \rightarrow 2CH_3OCH_2O + O_2$	$(3.0 \pm 2.1) \times 10^{-13}$ $\exp((700 \pm 250)/T)$	this work
4b	$CH_3OCH_2O_2 + CH_3OCH_2O_2 \rightarrow CH_3OC(O)H + CH_3OCH_2OH + O_2$		
21	$CH_3OCH_2O_2 + CH_3OCH_2 \rightarrow 2CH_3OCH_2O$	5×10^{-11}	est.[b]
	$CH_3OCH_2O_2 + OH \rightarrow CH_3OCH_2OH + O_2$	2×10^{-10}	est.[b]
	Alkoxy Radical Reactions		
5	$CH_3OCH_2O + M \rightarrow CH_3OC(O)H + H + M$	3×10^5 s^{-1}	this work
6	$CH_3OCH_2O + O_2 \rightarrow CH_3OC(O)H + HO_2$	$6 \times 10^{-14} \exp(-550/T)$	est.[b]
	H and HO_2 Radical Reactions		
15	$H + Cl_2 \rightarrow Cl + HCl$	$1.4 \times 10^{-10} \exp(-590/T)$	33
22	$H + CH_3OCH_2O_2 \rightarrow CH_3OCH_2O + OH$	5×10^{-10}	est.[b]
23a	$HO_2 + CH_3OCH_2O_2 \rightarrow CH_3OCH_2OOH + O_2$	$3.3 \times 10^{-13} \exp(800/T)$	30, 34
23b	$HO_2 + CH_3OCH_2O_2 \rightarrow CH_3OC(O)H + H_2O + O_2$	$2.7 \times 10^{-13} \exp(800/T)$	30
25	$H + O_2 + M \rightarrow HO_2 + M$	$5.7 \times 10^{-32}(T/298)^{-1.6}P_{tot}$	35
	$H + HO_2 \rightarrow OH + OH$	$2.8 \times 10^{-10} \exp(-440/T)$	36
	$HO_2 + HO_2 \rightarrow HOOH + O_2$	$2.8 \times 10^{-13} \exp(594/T)$	
	$HO_2 + OH \rightarrow H_2O + O_2$	$4.8 \times 10^{-11} \exp(250/T)$	35
	$HO_2 + HC(O)H \rightarrow HOCH_2OO$	$6.7 \times 10^{-15} \exp(600/T)$	35
	Methyl Radical Reactions		
	$CH_3 + O_2 + M \rightarrow CH_3O_2 + M$	$4.5 \times 10^{-31}(T/298)^{-3}P_{tot}$	35
	$CH_3O_2 + CH_3O_2 \rightarrow O_2 + 2CH_3O$	$(1\text{-}b) \times 9.1 \times 10^{-14} \exp(416/T)$	37
	$CH_3O_2 + CH_3O_2 \rightarrow O_2 + CH_3OH + HC(O)H$	$b(9.1 \times 10^{-14} \exp(416/T))$ $b = (1 + 25 \exp(-1165/T))^{-1}$	37
	$CH_3O_2 + CH_3OCH_2O_2 \rightarrow O_2 + CH_3O + CH_3OCH_2O$	4.5×10^{-12}	est.[b]
	$CH_3O_2 + CH_3OCH_2O_2 \rightarrow O_2 + HC(O)H + CH_3OCH_2OH$	7.5×10^{-13}	est.[b]
	$CH_3O_2 + CH_3OCH_2O_2 \rightarrow O_2 + CH_3OH + CH_3OC(O)H$	7.5×10^{-13}	est.[b]
	$CH_3O + O_2 \rightarrow HC(O)H + HO_2$	$7.2 \times 10^{-14} \exp(-1080/T)$	30
	Secondary Chemistry		
	$HC(O)H + OH \rightarrow HC(O) + H_2O$	$1.66 \times 10^{-11} \exp(-86/T)$	38
	$HC(O)H + H \rightarrow HC(O) + H_2$	$2.1 \times 10^{-12} \exp(-1090/T)$	39
	$HC(O)H + Cl \rightarrow HC(O) + HCl$	$8 \times 10^{-11} \exp(-30/T)$	35
	$HC(O) + O_2 \rightarrow HO_2 + CO$	$3.5 \times 10^{-12} \exp(140/T)$	35
26a	$CH_3OC(O)H \rightarrow CH_3OH + CO$	$8.3 \times 10^{10}T \exp(-37\,650/T)$ s^{-1}	this work
26b	$CH_3OC(O)H \rightarrow 2HC(O)H$	$1.9 \times 10^{10}T \exp(-40\,400/T)$ s^{-1}	this work
	$HOCH_2OO + HOCH_2OO \rightarrow 2HOCH_2O + O_2$	5.5×10^{-12}	27
	$HOCH_2OO + HOCH_2OO \rightarrow HC(O)OH + CH_2(OH)_2 + O_2$	$5.7 \times 10^{-14} \exp(750/T)$	27
	$HOCH_2OO + HO_2 \rightarrow$ products ($HOCH_2O_2H + O_2$)	$5.6 \times 10^{-15} \exp(2300/T)$	27
	$HOCH_2O + O_2 \rightarrow HC(O)OH + HO_2$	3.5×10^{-14}	40
	$HOCH_2O \rightarrow HC(O)OH + H$	$1.0 \times 10^{14} \exp(-7502/T)$ s^{-1}	41

[a] Reaction numbers are based on the sequence in the text. [b] Rate constants are based on estimates from analogous reactions as listed in the NIST chemical kinetics database (ref 27).

concentrations. However, these DME thermal oxidation measurements provide data needed to account for DME losses and product formations taking place in the reactor cell prior to initiation of the chemistry in the photolysis experiments reported below.

B. Photolysis-Initiated Kinetics Measurements. The photoinitiated kinetics measurements were performed to determine the branching ratio (f) of the $CH_3OCH_2 + O_2$ reaction pathways. Results from these measurements improve our understanding of the pressure dependent relaxation versus pressure independent dissociation of the activated methoxymethyl peroxy radical (reactions 3a and 3b), the temperature dependent rate constant expression of the peroxy self-reaction (reactions 4a and 4b), and the fate of the methoxymethyl alkoxy radical (reactions 5 and 6). The following time-resolved kinetics experimental results are discussed in terms of the proposed reaction mechanism in Table 1. The chemical reactions were carefully chosen to represent the experimental conditions under study. Outside our temperature and time regimes, other sets of reactions and pathways will start to play a role. $R + O_2$ chemistry will increase in complexity at combustion temperatures, as treated by Dryer et al.[24]

Branching Ratio of Alkyl Radical + O_2. The temperature and pressure dependence of the $CH_3OCH_2 + O_2$ branching ratio is determined from measurements of the real-time formation of formaldehyde and methyl formate over the first 100 μs following the Cl-initiated chemistry. Measurements are made at three pressures, referred to as low, medium, and high. It is the corresponding number densities of 65, 250, and 650 $\times$ 10^{16} molecules/cm^3 that are kept constant at the various measurement

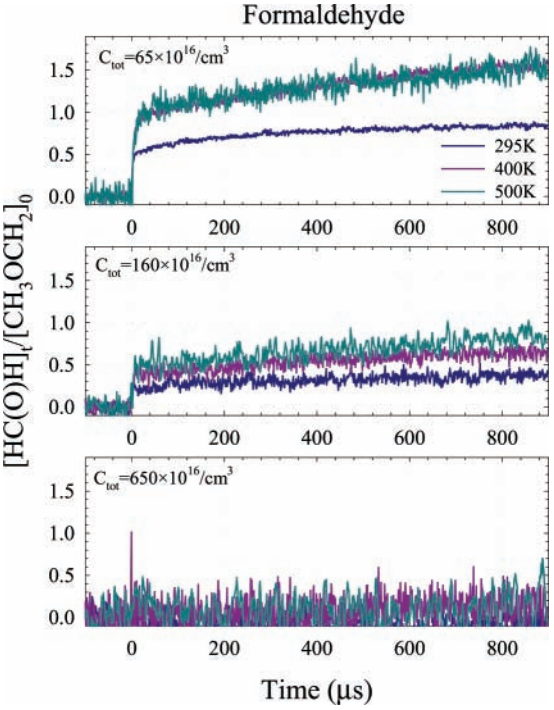

Figure 6. Formaldehyde concentration vs time profile from Cl-initiated DME degradation as a function of total pressure and temperature.

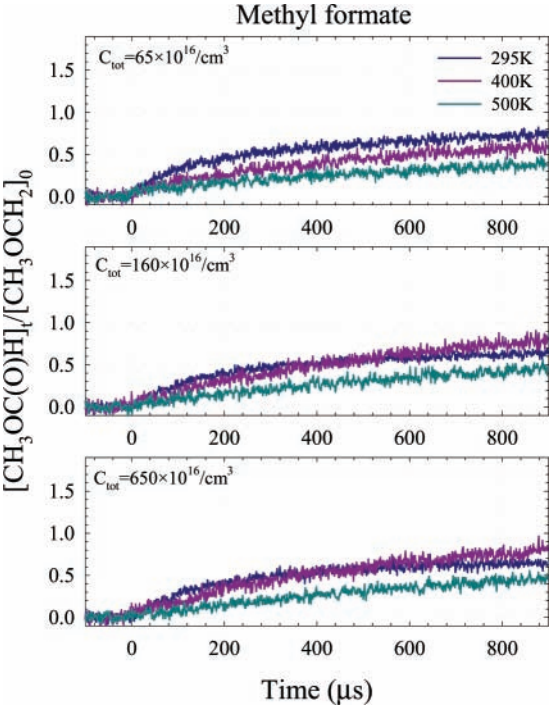

Figure 7. Methyl formate concentration vs time profile from Cl-initiated DME degradation as a function of total pressure and temperature.

temperatures. Figures 6 and 7 show the concentration profiles of formaldehyde and methyl formate versus time from $t = 0$ when the laser is fired up to 900 μs after photolysis, at 295, 400, and 500 K. The concentrations have been normalized with respect to the initial CH_3OCH_2 radical concentration produced by the photolysis of Cl_2. Due to the high initial radical concentrations for these measurements, $>10^{14}$/cm^3, the DME degradation chemistry proceeds rapidly, and therefore, the products are monitored only for the first 900 μs after the chemistry is initiated by chlorine atoms.

Unlike the products observed from thermal decomposition, measurable concentrations were not obtained for formic acid. Two distinctive and competitive pathways lead to the formation of formaldehyde and methyl formate. To recall, the proposed mechanism shows that formaldehyde is produced from the pressure independent pathway and methyl formate is produced from the pressure dependent pathway.

$$CH_3OCH_2 + O_2 \rightarrow CH_3OCH_2O_2^* + M \rightarrow CH_3OCH_2O_2 + M \quad (3a)$$

$$CH_3OCH_2 + O_2 \rightarrow CH_3OCH_2O_2^* \rightarrow CH_2OCH_2O_2H \rightarrow 2HC(O)H + OH \quad (3b)$$

$$2CH_3OCH_2O_2 \rightarrow 2CH_3OCH_2O + O_2 \quad (4a)$$

$$2CH_3OCH_2O_2 \rightarrow CH_3OC(O)H + CH_3OCH_2OH + O_2 \quad (4b)$$

The formation of formaldehyde (Figure 6) is characterized by a rapid initial rise during the first 10 μs, a characteristic of primary chemical reactions, and is due to the fraction of peroxy radicals that undergo dissociation. Beyond 10 μs, the rise in formaldehyde concentration levels off and is due to the H atoms generated from the decomposition of the alkoxy radical. This initiates a chain reaction that is sustained as DME undergoes hydrogen abstraction, producing fresh alkyl radicals.

$$CH_3OCH_2O + M \rightarrow CH_3OC(O)H + H + M \quad (5)$$

$$H + Cl_2 \rightarrow Cl + HCl \quad (15)$$

$$CH_3OCH_3 + Cl \rightarrow CH_3OCH_2 + HCl \quad (2)$$

At room temperature, the formaldehyde yield levels off after a few hundred microseconds, but at higher temperatures, it continues to rise for a longer time. The yield increases with increasing temperature and decreases with increasing pressure. IR absorption detection becomes increasingly difficult as the total pressure is increased. The signal-to-noise ratio and sensitivity degrade with pressure due to the smaller product concentrations and the pressure broadening effect on the absorbance cross section.

In contrast, the initial methyl formate concentration starts to rise gradually shortly after $t = 0$ (Figure 7), a characteristic of secondary product formation. The production of methyl formate is the result of the methoxymethyl peroxy radical self-reaction and the decomposition of the methoxymethyl alkoxy radicals, accounting for approximately 95% of the methyl formate concentration (reactions 4 and 5). The rate of methyl formate formation is determined by the overall removal rate of the methoxymethyl peroxy radical. It has a weak dependence on temperature and pressure, being slightly enhanced at higher temperature and lower pressure conditions. IR detection of methyl formate is not sensitive to changes in total pressure because its absorbance spectrum is effectively fully pressure broadened and remains nearly constant over the pressure range of interest. The lack of detectable concentrations of formic acid indicates that it is not a primary or even a secondary product of the methoxymethyl peroxy radical chemistry. However, since formic acid is observed as a thermal degradation product while the DME/O_2 mixture is in the heated reactor cell for 2−4 s, it must be produced from subsequent reactions, albeit at a much slower rate than could be monitored in these kinetics experiments.

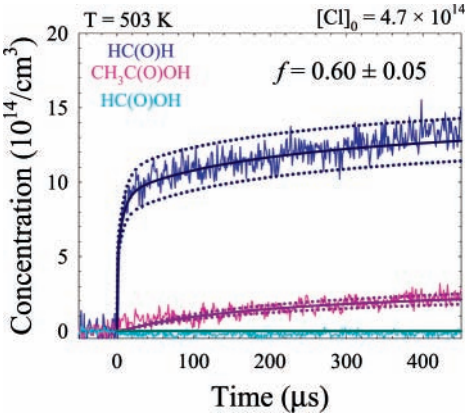

Figure 8. Formaldehyde, methyl formate, and formic acid yields vs time for the first 450 μs at 503 K and 60 × 10^{16} molecules/cm^3.

The photoinitiated oxidation of dimethyl ether is proposed to proceed via the mechanism listed in Table 1, consisting of 34 chemical reactions. Published rate constants for the reactions in the mechanism are provided. Rate constants based on analogous methyl or ethyl radical reactions of known reported values are used as estimates for reactions where literature values are not available. The reaction mechanism is cast into a coupled set of differential equations and is numerically solved using the Scientist software, version 2.02 (Micromath, Inc). To determine the branching ratio of reaction 3, the calculations are propagated over the first 100 μs following the flash photolysis, which minimizes interference from the secondary reactions. The branching ratio (f) and the initial concentration of Cl atoms produced by laser photolysis are simultaneously determined when performing fits to the data. Figure 8 shows the formaldehyde, methyl formate, and formic acid yields at a temperature of 503 K and under low-pressure conditions. The solid line through the experimental data trace represents the predicted product yield when fitting the model simultaneously to the measured formaldehyde and methyl formate concentrations. The dotted lines represent the changes in the predicted product yield when the branching ratio is varied by ±8%. Because of this sensitivity, the formaldehyde yield provides an accurate measure of the branching ratio of the $CH_3OCH_2 + O_2$ reaction.

The kinetics of methoxymethyl peroxy radical formation can be described by the Lindemann−Hinshelwood theory. The modified Lindemann mechanism applicable to this work is described by reactions 3a and 3b. Once the excited methoxymethyl peroxy radical ($CH_3OCH_2O_2$*) is produced, it can undergo collisional relaxation or dissociation. Maricq et al.[13] parametrized the pressure dependence of these two pathways as

$$k_{\text{relaxation}} = k_{3a} = \frac{k_{\text{ro2,0}}[\text{M}]}{1 + (k_{\text{ro2,0}}[\text{M}]/k_{\text{ro2,}\infty})} \tag{16}$$

$$k_{\text{dissociation}} = k_{3b} = \frac{k_{\text{HC(O)H,0}}}{1 + (k_{\text{ro2,0}}[\text{M}]/k_{\text{ro2,}\infty})} \tag{17}$$

where $k_{\text{ro2,0}}$ depends on the nature of the bath gas M (in this case N_2), $k_{\text{ro2,}\infty}$ is the high-pressure limit for peroxy formation, and $k_{\text{HC(O)H,0}}$ is the rate constant for the dissociation pathway. The overall rate constant for the removal of CH_3OCH_2 radicals by O_2 is

$$k_{\text{ro2}} = k_{\text{relaxation}} + k_{\text{dissociation}} = \frac{k_{\text{HC(O)H,0}} + k_{\text{ro2,0}}[\text{M}]}{1 + (k_{\text{ro2,0}}[\text{M}]/k_{\text{ro2,}\infty})} \tag{18}$$

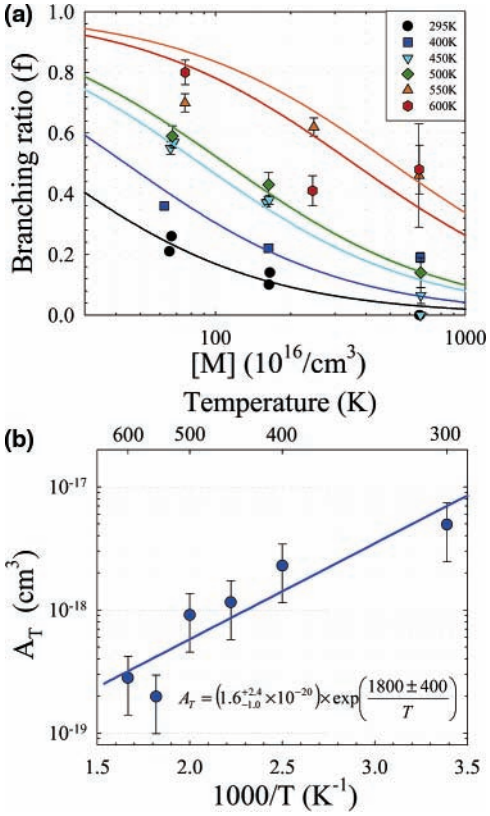

Figure 9. (a) Branching ratio (f) as a function of temperature and pressure (symbols, experimental results; solid line, prediction from fit to eq 19). (b) Temperature dependence of A_T.

The resulting branching ratio (f) for the formaldehyde channel is given by

$$f = \frac{k_{\text{dissociation}}}{k_{\text{ro2}}} = \frac{1}{1 + A_T[\text{M}]} \tag{19}$$

where A_T is defined as the ratio of $k_{\text{ro2,0}}/k_{\text{HC(O)H,0}}$ and [M] represents the total concentration.

Figure 9a compares the measured branching ratios to the pressure dependence given by eq 19. At room temperature, the branching ratio is approximately 0.2 at a number density of 65 × 10^{16} molecules/cm^3 (20 Torr) and 0.0 at number densities above 650 × 10^{16} molecules/cm^3 (200 Torr). At 500 K, the branching ratio increases to 0.6 at low pressure and is 0.14 at high pressure. At 600 K, it appears that the branching ratio begins to decrease; however, by this temperature, the interference from thermal degradation of DME is becoming significant, so this decrease might not be reliable.

Values for A_T are calculated at each temperature by fitting eq 19 to the pressure dependent branching ratios, shown by the lines in Figure 9a. These are plotted against temperature in Figure 9b. A_T shows a negative temperature dependence, decreasing exponentially as the temperature increases. Since A_T represents the ratio of rate constants for the two competitive pathways for the $CH_3OCH_2 + O_2$ reaction, we expect it to exhibit an Arrhenius dependence. The fit of the data in Figure 9b (solid line) yields

$$A_T = (1.6^{+2.4}_{-1.0} \times 10^{-20}) \exp\left(\frac{1800 \pm 400}{T}\right) \text{cm}^3 \text{ molecule}^{-1} \tag{20}$$

Overall, the expressions for f and A_T show that the dissociation

path for the methoxymethyl + O_2 reaction is greater with increasing temperature but becomes smaller with increasing pressure.

$CH_3OCH_2O_2$ Self-Reaction. Once methoxymethyl peroxy radicals form, their primary fate under these experimental conditions is removal via self-reaction. Methyl formate is the main product from both branches of the peroxy self-reaction, either as a direct product (reaction 4b) or from the degradation of the methoxymethyl alkoxy radical (reactions 5 and 6).

$$2CH_3OCH_2O_2 \rightarrow 2CH_3OCH_2O + O_2 \quad (4a)$$

$$2CH_3OCH_2O_2 \rightarrow CH_3OC(O)H + CH_3OCH_2OH + O_2 \quad (4b)$$

$$CH_3OCH_2O + M \rightarrow CH_3OC(O)H + H + M \quad (5)$$

$$CH_3OCH_2O + O_2 \rightarrow CH_3OC(O)H + HO_2 \quad (6)$$

The competition between reactions 5 and 6 in removing alkoxy radicals will be addressed in the next section. A pressure independent rate constant for the peroxy self-reaction was reported by Jenkin et al. to be $(2.1 \pm 0.3) \times 10^{-12}$ cm^3 molecule^{-1} s^{-1} at 298 K with a branching ratio of 0.7 ± 0.1 in favor of reaction 4a.[15] In the present study, kinetics data for HC(O)H and $CH_3OC(O)H$ formation during the first 500 μs following the photoinitiated production of methoxymethyl peroxy radicals is used to calculate the temperature dependent self-reaction rate constant (k_4). Since both pathways of the peroxy self-reaction lead to methyl formate production, it was not feasible to determine the branching ratio for reactions 4a and 4b.

The same kinetics model is used as described in the previous discussion on CH_3OCH_2 + O_2 chemistry (Table 1). One modification is that the values for the pressure and temperature dependent alkyl + O_2 branching ratio (f) are incorporated into the model. The methoxymethyl peroxy self-reaction rate constant is calculated using data from the high-pressure conditions, $\approx 650 \times 10^{16}$ molecules/cm^3, over the temperature range 295−600 K. At the higher pressure, very little, if any, of the peroxy radicals undergo dissociation and therefore the initial production of peroxy radicals is not impacted by reaction 3b (dissociation into formaldehyde and hydroxyl radicals). In addition to the peroxy self-reaction, several other reactions can contribute to methyl formate production. They include

$$CH_3OCH_2O_2 + CH_3OCH_2 \rightarrow 2CH_3OCH_2O \quad (21)$$

$$H + CH_3OCH_2O_2 \rightarrow CH_3OCH_2O + OH \quad (22)$$

$$HO_2 + CH_3OCH_2O_2 \rightarrow CH_3OC(O)H + H_2O + O_2 \quad (23b)$$

However, these reactions contribute less than 10% to the total amount of methyl formate production. The measured values for the peroxy self-reaction rate constant (k_4) are plotted against $1/T$ in Figure 10. The solid line in this figure represents the Arrhenius temperature dependence.

$$k_4 = (3.0 \pm 2.1) \times 10^{-13} \exp\left(\frac{700 \pm 250}{T}\right) \text{cm}^3 \text{ molecule}^{-1} \text{ s}^{-1} \quad (24)$$

At 298 K, $k_4 = 3.1 \times 10^{-12}$ cm^3 molecule^{-1} s^{-1}, which is consistent with the value obtained by Jenkin et al.[15] The activation energy $E_a/R = -700$ K indicates a weak negative temperature dependence. This property is typical of peroxy self-reaction rate constants, as shown in Table 2. The large error bars for k_4 (Figure 10) arise in part from the indirect measurement of the peroxy self-reaction by monitoring the byproducts, mainly methyl formate and formaldehyde. Nevertheless, the results are consistent with previously reported values and provide a reasonable estimate for the temperature dependence of this rate constant.

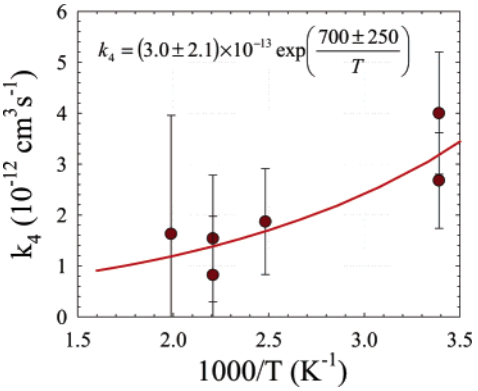

Figure 10. Temperature dependence of the $CH_3OCH_2O_2$ self-reaction rate constant at high pressure (650×10^{16}/cm^3).

TABLE 2: Comparison of Self-Reaction Rate Constants for Several Peroxy Radicals

RO_2	k_{298}[a]	k_T[a]	temperature range (K)	ref
CH_3O_2	3.7×10^{-13}	$9.1 \times 10^{-14} \exp(416/T)$	248−650	37
HO_2	2.1×10^{-12}	$2.8 \times 10^{-13} \exp(594/T)$	210−263	42
$CH_3C(O)O_2$	1.6×10^{-11}	$3.0 \times 10^{-12} \exp(504/T)$	209−358	43
$HOCH_2O_2$	7.0×10^{-13}	$5.65 \times 10^{-14} \exp(750/T)$	275−323	44
$CH_3OCH_2O_2$	2.1×10^{-12}	n.a.	298	15
	3×10^{-12}	$3.0 \times 10^{-13} \exp(700/T)$	295−600	this work

[a] Rate constant units are cm^3 molecule^{-1} s^{-1}.

Fate of the Methoxymethyl Alkoxy Radical (Decomposition vs Reaction with O_2). In the course of applying the kinetics model to determine the branching ratio for the CH_3OCH_2 + O_2 reaction as well as the $CH_3OCH_2O_2$ self-reaction rate constant, it was necessary to examine the fate of the methoxymethyl alkoxy radical (CH_3OCH_2O) and its impact on the formation of formaldehyde and methyl formate. Methoxymethyl alkoxy radicals are mainly produced from the methoxymethyl peroxy radical. Once formed, the alkoxy radical is expected to either undergo unimolecular decomposition or react with O_2 to produce methyl formate. In the previous study by Jenkin et al.,[15] FTIR spectroscopy was used to investigate the methoxymethyl peroxy radical self-reaction rate constant. The methoxymethyl peroxy radical removal rate is influenced by the formation of either H atoms or HO_2 radicals from the alkoxy radical decompostion or its reaction with O_2, respectively. HO_2 promotes the removal of peroxy radicals, while H atoms may indirectly generate additional peroxy radicals through the Cl atoms produced by the H + Cl_2 reaction. From the observed rapid enhancement of the peroxy self-reaction at a total pressure of 25 Torr and 298 K, it was concluded that H atom ejection from the methoxymethyl alkoxy radical occurs preferentially to its reaction with O_2, since the final product yields were dependent on the competition between O_2 and Cl_2 for the H atoms produced by methoxymethyl alkoxy decomposition.

As part of the present study, the kinetics of HC(O)H and methyl formate formation provide insight into the competition between the methoxymethyl alkoxy radical decomposition and its reaction with oxygen (reactions 5 and 6). Whereas both

reactions convert the alkoxy radical to methyl formate, the decomposition reaction also produces H atoms while reaction with O_2 produces HO_2 radicals. For these kinetic experiments, it was necessary to keep the O_2 concentration at or above 65×10^{16} molecules/cm^3 to ensure that the main fate of the methoxymethyl radical is to react with oxygen (reactions 3a and 3b). This requirement prevented the use of lower O_2 concentrations that might have influenced the competition between reactions 5 and 6. The importance of H atom production under our experimental conditions is the capability to sustain a chain reaction with dimethyl ether. H atoms can react with available Cl_2 to produce Cl atoms, which in turn are a source of new methoxymethyl radicals.

$$CH_3OCH_2O + M \rightarrow CH_3OC(O)H + H + M \quad (5)$$

$$H + Cl_2 \rightarrow HCl + Cl \quad (15)$$

$$Cl + CH_3OCH_3 \rightarrow CH_3OCH_2 + HCl \quad (2)$$

$$H + CH_3OCH_2O_2 \rightarrow CH_3OCH_2O + OH \quad (22)$$

$$OH + CH_3OCH_3 \rightarrow CH_3OCH_2 + H_2O \quad (13)$$

$$H + O_2 + M \rightarrow HO_2 + M \quad (25)$$

A sensitivity analysis performed on the $H + Cl_2$ reaction indicates that approximately 60% of the H atoms are lost through the reaction with Cl_2 (reaction 13) and that another 30−35% are consumed by the reaction with peroxy radicals (reaction 22), to produce alkoxy and OH radicals. OH radicals react very efficiently with DME to generate fresh methoxymethyl radicals. Other minor reactions for the H atoms are direct reaction with DME (reaction 14) and reaction with O_2 to make HO_2 radicals (reaction 25). In contrast, if the alkoxy radical reacts with molecular oxygen (reaction 6), the produced HO_2 will mainly react with the peroxy radical.

$$CH_3OCH_2O_2 + HO_2 \rightarrow CH_3OCH_2OOH + O_2 \quad (23a)$$

$$\rightarrow CH_3OC(O)H + H_2O + O_2 \quad (23b)$$

Reaction 23 is effectively a termination step because HO_2 cannot propagate the chain reaction and instead enhances the rate at which methoxymethyl peroxy radicals are removed. However, this is a very minor path for the alkoxy, since reaction 23b accounts only for 2% of the observed methyl formate concentration.

The different pathways for reactions 5 and 6 influence the rate of formaldehyde formation during the time period when most of the peroxy radical is being lost, 20−500 μs following laser photolysis. The kinetics model described by Table 1 is utilized to evaluate reactions 5 and 6 by tracking the formaldehyde formation over the 400 μs period following its initial production via the photoinitiated radicals and solving for k_5, the unimolecular decomposition rate constant of the alkoxy radical. The rate constant for the alkoxy + O_2 reaction (k_6) is assigned a value of $6 \times 10^{-14} \exp(-550/T)$ cm^3 molecule^{-1} s^{-1} which is based on the analogous ethoxy + O_2 reaction.[27] Figure 11 shows the formaldehyde and methyl formate concentrations at 503 K and at low pressure ($f = 0.6$). The solid line represents the predicted product yields for $k_5 = 2 \times 10^5$ s^{-1} where the alkoxy dissociation accounts for 96% of its removal. The dashed line shows the change in these product yields when k_5 is reduced by a factor of 10 to 2×10^4 s^{-1} which reduces the fraction of alkoxy that dissociates to 70%.

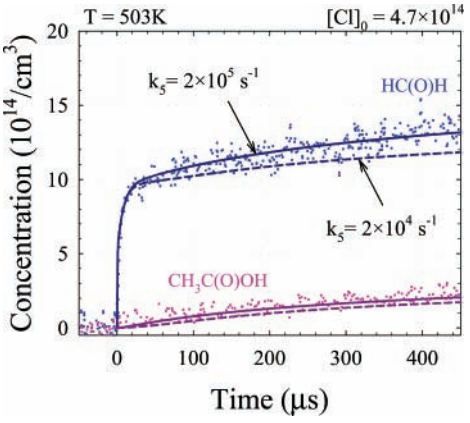

Figure 11. Branching ratio of methoxymethyl alkoxy radical dissociation vs oxygen addition at 503 K and 60×10^{16} molecules/cm^3.

For this case, the model is clearly underestimating the production of formaldehyde after the first 20 μs. This effect is apparent, but noticeably smaller, on the predicted methyl formate concentration. The continued production of H atoms by reaction 5 accounts for the gradual rise in formaldehyde concentration for times between 50 and 450 μs. The value selected for k_5, 2×10^5 s^{-1}, is a lower limit for the rate constant, since the rate-limiting reaction for these products is the methoxymethyl peroxy self-reaction (reaction 4).

C. Theoretical Determination of the Methyl Formate Thermal Decomposition Rate Constant. The kinetics model in Table 1 assumes that there is no significant removal of methyl formate. However, the thermal decomposition of methyl formate presents a potential loss mechanism. To investigate this possibility, the temperature dependent rate constants of two possible methyl formate decomposition pathways have been determined theoretically.

$$CH_3OC(O)H \rightarrow CH_3OH + CO \quad (26a)$$

$$CH_3OC(O)H \rightarrow 2HC(O)H \quad (26b)$$

Francisco[28] proposed that methyl formate decomposition proceeds mainly through reactions 26a and 26b. Ab initio molecular orbital calculations performed on methyl formate and the transition state structures were used to describe the energetics of the potential energy surface for the unimolecular decomposition pathways of methyl formate, and Rice−Ramsperger−Kassel−Marcus (RRKM) calculations determined the unimolecular microcanonical dissociation rates as a function of internal energy. Equilibrium geometries and vibrational frequencies were found using the second-order Møller−Plesset perturbation method (MP2) with a 6-311G(2df,2p) basis set. This work suggested that methyl formate thermal decomposition takes place via two competitive parallel reactions forming $CH_3OH + CO$ and $HC(O)H + HC(O)H$, with activation energies of 74.8 and 80.3 kcal/mol and heats of reaction of 8.5 and 30.6 kcal/mol, respectively. The activation barriers of these two channels are below the bond fission energy requirements in methyl formate, the CH bond on the carbonyl group (92.7 kcal/mol) and the CH bond on the methyl group (100 kcal/mol).

In the present study, the prior ab initio results were reevaluated to describe the thermochemistry and kinetics of these two channels (reactions 26a and 26b) during methyl formate thermal decomposition. The rate constant (k) for each channel is calculated from transition state theory, given by

$$k = \frac{LTk_b}{h}\frac{Q_{transitionstate}}{Q_{methylformate}}e^{-E_a/RT} \quad (27)$$

where L is the degeneracy factor, T is the temperature in kelvins, k_b is Boltzmann's constant, h is Plank's constant, R is the gas constant, E_a is the activation energy between transition state and reactant, including zero point energy correction, and Q is the total partition function incorporating translational, rotational, vibrational, and electronic contribution ($Q_T = Q_tQ_rQ_vQ_e$). An expression of the rate constant as a function of temperature is obtained. The carbonyl CH bond fission and consequent production of $CH_3OH + CO$ is estimated to have a temperature dependent rate constant of $k_{26a} = 8.3 \times 10^{10}T \exp(-37\,650/T)$ s^{-1}, while the methyl CH bond fission with the formation of two HC(O)H proceeds with a temperature dependent rate constant of $k_{26b} = 1.9 \times 10^{10}T \exp(-40\,400/T)$ s^{-1}. These rate constants represent high-pressure limits. These values were incorporated in the kinetics model to account for the potential significance of methyl formate thermal decomposition at the temperatures examined in this study. Over the temperature range 295−700 K, thermal decomposition is not responsible for methyl formate removal.

D. Error Analysis. *Experimental Measurements.* The sources of measurement uncertainty are determined as follows. The reactor flow cell length has ±1% uncertainty (48 ± 0.5 cm). The total pressure in the reactor flow cell was determined by taking the average of pressure readings at both ends of the cell. The accuracy of MKS pressure gauges is better than ±1%; however, the pressure drop between the entry and exit points for the gases produced at most a 10% gradient in pressure along the length of the reactor cell, leading to a ±5% uncertainty in the average pressure. Due to the temperature gradient at the ends of the reactor cell, uncertainty in the temperature is expected to increase as it is raised from room temperature. The interior temperature of the reactor was checked in separate measurements with a thermocouple inserted along the axis of the flow cell and with nitrogen flowing to simulate the flow rate and total pressures for the kinetics experiments, and it was found that the temperature inside remained within 10 K of the external temperature along 90% of the length. Temperature gradients of Δ5 K at 400 K and Δ10 K at 700 K were observed. For the DME oxidation measurements, multiple thermocouples (±1% accuracy on each), positioned on the outside of the flow cell, were utilized to monitor the temperature. The combination of these factors results in an uncertainty of ±2% in the temperature of the gas mixture. Uncertainties in the individual gas concentrations derive from the total pressure and flow rates. Their combined uncertainty in the individual gas concentrations is estimated to be ±6%.

The photolysis laser energy variability contributes to uncertainty in the initial Cl radical concentration. The excimer laser energy varies a maximum of ±10% from pulse to pulse, but since each measurement was the average of at least 100 pulses, the overall variation in the laser energy is less than ±1%. The tunable diode laser IR frequency of the selected absorbance lines can be reported within ±0.5 cm^{-1} on the basis of the accuracy of the mode selection monochromator on the diode laser apparatus. The IR beam was amplitude modulated with a mechanical chopper to measure absolute intensities and had an accuracy of ±1 mV or better based on the 12 bit resolution of the digital oscilloscope and signal averaging. The typical variability in the IR absorption measurements is estimated to be around ±2% on the basis of the inherent noise in the IR diode laser output as well as the IR detector preamplifier.

To measure IR cross sections, reference gas mixtures are prepared by incremental dilution in glass flasks which have the same sources of uncertainty as the flow rate measurements described above. The respective reference gas concentration is reported within ±6%. Uncertainties in cross sections increase due to pressure broadening. Weaker absorbances increase the signal-to-noise ratios which were partially overcome by increasing the concentration of the reference gas. The combination of the measurement uncertainties yields no more than ±10% uncertainty in the IR cross sections.

Kinetics Model. The kinetics data reported in this work are derived by comparing observations to the reaction model in Table 1. Uncertainties in the published or estimated rate constants therefore contribute to the uncertainty in the data reported here. The extent of that uncertainty is examined using a sensitivity analysis approach. From the sensitivity analysis, only reaction 13 (DME + OH) and reaction 3 ($CH_3OCH_2 + O_2$) produce noticeable changes in f and Cl_0 when their rate constants are adjusted by the listed uncertainties, resulting in ±10% uncertainty in Cl_0 when k_{13} is varied and ±2% in both f and Cl_0 when k_3 is varied. The remaining reactions have either secondary or tertiary effects on the formaldehyde and methyl formate formation during the first 50−100 μs, so their rate constants are not a factor in determining f or Cl_0. The effects of uncertainties in the initial conditions (i.e., individual gas pressures and temperature) on the branching ratio (f) were evaluated under the experimental time regime and temperature conditions. A variation of ±10% in Cl_0 resulted in a maximum change of ±5% in f. When the initial DME concentration was varied by ±20%, a change of ±5% in Cl_0 and < ±1% in f was observed. Changes of ±20% in O_2 concentration produced approximately a change of ±1% in the branching ratio and initial chlorine concentration. No effect was observed on f and Cl_0 when the total pressure was changed by ±10%. A ±20% change in Cl_2 concentration resulted in a less than 1% change in Cl_0 and f. Variation of the temperature did not produce any effect on the predictions of these two parameters. The variation on the time dependent concentrations of formaldehyde and methyl formate by ±10% yields an overall uncertainty of ±8% on the branching ratio and ±10% on the initial chlorine concentration.

Discussion & Conclusion

The degradation of dimethyl ether has been investigated in detail at temperatures of 295−700 K and total concentrations of (65−650) × 10^{16} molecules/cm^3. The yields of three products—formaldehyde, methyl formate, and formic acid—were monitored by flash photolysis/time-resolved IR spectroscopy in the carbonyl stretch region 1700−1800 cm^{-1}. Thermal degradation measurements provided information about the extent of DME losses as well as the concentrations of these products at temperatures above 500 K. The results from these measurements are similar to the trend observed by Liu et al.[26] in the removal of DME over this temperature range. Consumption of DME in the presence of oxygen is enhanced as the temperature is raised to 650 K. Above 650 K, the reduction in the concentrations of degradation products indicates that the DME oxidation is entering a negative temperature coefficient region. Andersen et al.[18] used density functional theory to show that the formation of the rearranged peroxy radical, CH_2OCH_2OOH, and its subsequent secondary chemistry is responsible for the DME autoignition properties. An additional consideration is that, as the temperature is further increased, dimethyl ether decomposition ($CH_3OCH_3 \rightarrow CH_3O + CH_3$) and the DME + O_2 reaction will dominate the initial DME kinetics.[21−23] The fate of the

methoxymethyl radical also changes as its decomposition ($CH_3OCH_2 \rightarrow CH_3 + HC(O)H$) becomes a significant reaction which will determine to a large extent the final products in the combustion regime.[17] All of these factors will interfere with the $CH_3OCH_2 + O_2$ reaction, which was the primary focus of this study. As such, it was necessary to carry out the experiments at temperatures below 700 K to obtain reliable kinetics measurements of this DME degradation pathway.

In the previous study by Maricq et al.,[13] a temperature dependent trend in the branching ratio (f) was observed for the $CH_3OCH_2 + O_2$ reaction up to 350 K and 100 Torr. On the basis of only formaldehyde yields during the first 80 μs after chlorine photolysis, they observed a shift in the branching ratio from $f = 0.37$ at 230 K to $f = 0.52$ at 350 K at a total pressure of 10 Torr. Since the results were limited by the narrow temperature and pressure ranges and the detection of the formaldehyde product only, the present study was carried out to examine this reaction over a broader range of temperatures and pressures to determine the importance of the OH radical production from $CH_3OCH_2 + O_2$ during ignition of DME.

The photoinitiated kinetics of the $CH_3OCH_2 + O_2$ reaction was characterized to determine the temperature and pressure dependence of the branching ratio of the methoxymethyl peroxy radical dissociation versus relaxation. The results were analyzed by comparing the formaldehyde and methyl formate product yields to those predicted by the reaction mechanism of DME oxidation in Table 1. The branching ratio has been shown to increase as the temperature increases and the pressure decreases and has been calculated using Lindemann and Arrhenius analysis by the following expression: $f = 1/(1 + A_T[M])$, where $A_T = (1.6^{+2.4}_{-1.0} \times 10^{-20}) \exp((1800 \pm 400)/T)$ cm^3 molecule^{-1}. The formaldehyde yield provided an accurate way for the kinetics model to determine the $CH_3OCH_2 + O_2$ reaction branching ratio.

The dissociation of methoxymethyl peroxy radicals to produce OH radicals is significant because of their role in sustaining a chain reaction with DME. It is interesting to compare the dissociation pathway of the $CH_3OCH_2 + O_2$ reaction to the $C_2H_5 + O_2$ reaction. Ethyl radical (C_2H_5) reactions are used as models of other alkyl and peroxy radical reactions. Kaiser[29] has characterized the temperature and pressure dependence of the ethene (C_2H_4) yield from the $C_2H_5 + O_2$ reaction, which also undergoes dissociation and relaxation pathways similar to $CH_3OCH_2O_2$ radicals

$$C_2H_5 + O_2 \leftrightarrow C_2H_5O_2^* \tag{28}$$

$$C_2H_5O_2^* \rightarrow C_2H_4O_2H^* \rightarrow C_2H_4 + HO_2 \tag{29}$$

$$C_2H_5O_2^* + M \rightarrow C_2H_5O_2 + M \tag{30}$$

The HO_2 radicals produced by the dissociation pathway will either react with $C_2H_5O_2$ radicals or undergo self-reaction. This is in contrast to the OH radicals generated by the dissociation pathway of methoxymethyl peroxy radicals, which are excellent chain propagation intermediates. The $CH_3OCH_2 + O_2$ reaction is going to be sustained as long as OH radicals are produced which is not the case for the ethyl radicals.

The peroxy self-reaction (reaction 4) and the decomposition of the alkoxy radical (reaction 5) were also examined at these temperatures and pressures. The temperature dependent rate constant of the methoxymethyl peroxy radical self-reaction was calculated using the kinetics of the formaldehyde and methyl formate product yields, $k_4 = (3.0 \pm 2.1) \times 10^{-13} \exp((700 \pm 250)/T)$ cm^3 molecule^{-1} s^{-1}. The magnitude and temperature dependence of this rate constant are similar to those of the rate constants of other peroxy radical self-reactions. The methoxymethyl alkoxy radical decomposition was determined by the secondary formaldehyde formation from the peroxy radical self-reaction to be $k_5 > 2 \times 10^5$ s^{-1}. Jenkin et al.[15] obtained a rate constant of 3000 s^{-1} at 298 K for this decomposition reaction. Both results support a strong competition between the thermal decomposition of alkoxy radicals versus their reaction with O_2, resulting in the ejection of H atoms as the main fate of the methoxymethyl alkoxy radicals. The discrepancy between these two values for k_5 may be due to the fact that both methods were indirect determinations that monitored products from more than one reaction. It is expected that the alkoxy radical decomposition rate is temperature dependent, but that could not be determined by our experiments. This is due to the fact that the peroxy radical self-reaction is the rate-limiting step in the formation of methyl formate and formaldehyde at times longer than the initial 20 μs period following photolysis. Nevertheless, a lower limit for k_5 was determined from these product yields. A more direct method of studying this reaction would be needed to obtain this rate constant with more accuracy.

In terms of diesel fuel and combustion chemistry implications, as the temperature is increased, it is expected that the peroxy radical more readily undergoes thermal dissociation, which increases the rate at which methoxy methyl radicals get recycled through the activated RO_2* intermediate. Effectively, therefore, reaction 3b becomes more competitive. The temperature increase will affect the amount of OH radicals produced by channel 3b and consequently the net consumption of DME by chain reactions. At combustion temperatures of at least 1000 K, the decomposition of the methoxymethyl peroxy radical into formaldehyde and OH radicals is expected to be a major pathway. On the other hand, when the pressure dependence is considered along with the temperature effect, the scenario gets more complicated. The pressure effect on the branching ratio is more significant than the temperature effect. However, the enhanced fraction of RO_2* which undergoes dissociation is not significant enough to sustain a chain reaction at temperatures approaching DME ignition and combustion. As such, the reaction of $CH_3OCH_2 + O_2$ is not expected to be responsible for the good ignition properties observed during DME combustion. Due to the restrictions on the temperature and pressure ranges covered by this study and the fact that they are much lower than actual combustion temperatures and pressures, the results presented in this study may not be applicable to combustion conditions. It is expected that dimethyl ether decomposition, DME + O_2, and decomposition of the methoxymethyl radical are the significant reactions which will determine to a large extent the final products in the combustion regime.

The temperatures and pressures explored in this study resemble more closely those of SOFCs. H_2, CH_4, and CO are major species that have been identified previously in SOFCs from the decomposition of DME + O_2 mixtures at temperatures of 823 K.[8] SOFCs operated with DME in the presence of O_2 have been shown to generate more electric power at temperatures 50−100 K lower than when operating with pure DME. In the low-temperature regime, DME degradation would be initiated by O_2, accounting for at least half of the DME decomposition. Under SOFC operating conditions of 823 K and 1 atm, the branching ratio (eq 19) is expected to approach 50%. Under these conditions, the oxidation of DME can proceed mainly via the decomposition of peroxy radicals into OH radicals and formaldehyde. OH radicals might also play a role in the enhancement of the consumption of fuel by chain reactions in

SOFCs. The results from the present study, especially the trend in the branching ratio with respect to temperature and pressure, might provide insight into optimizing SOFC operating conditions with DME in the presence of O_2 to maximize power outputs. Also, lower operating temperatures would eliminate the need for an external reformer and will ensure stability and durability of the ceramic structure of a SOFC unit.

Acknowledgment. The authors would like to thank Bill Kaiser for his valuable insight and Michael Kamboures for his assistance in performing kinetics experiments.

References and Notes

(1) Leppard, W. R. *SAE Tech. Pap. Ser.* **1991**, *912313*.
(2) Kapus, P. E.; Cartellieri, W. P. *SAE Tech. Pap. Ser.* **1995**, *952754*.
(3) Fleisch, T.; McCarthy, C.; Basu, A.; Udovich, C.; Charbonneau, P.; Slodowske, W.; Mikkelsen, S.; McCandless, J. *SAE Tech. Pap. Ser.* **1995**, *950061*.
(4) Rouhi, A. M. *Chem. Eng News* **1995**, *44*, 37.
(5) Teng, H.; McCandless, J. C.; Schneyer, J. B. *SAE Tech. Pap. Ser.* **2001**, *010154*.
(6) Sehested, J.; Møgelberg, T.; Wallington, T. J.; Kaiser, E. W.; Nielsen, O. J. *J. Phys. Chem.* **1996**, *100*, 17218.
(7) Perry Murray, E.; Harris, S. J.; Jen, H. *J. Electrochem. Soc.* **2002**, *149*, A1127.
(8) Perry Murray, E.; Harris, S. J.; Liu, J.; Barnett, S. A. *Electrochem. Solid-State Lett.*, in press.
(9) Muller, J. T.; Urban, P. M.; Holderich, W. F.; Colbow, K. M.; Zhang, J.; Wilkinson, D. P. *J. Electrochem. Soc.* **2000**, *147*, 4058.
(10) Singhal, S. C. *MRS Bull.* **2000**, *3*, 16.
(11) Mikkelsen, S. H.; Hansen, J. B.; Sorenson, S. C. Dimethyl Ether as an Alternate Fuel for Diesel Engines. *Application of Powertrain & Fuel Technology to Meet Emission Standards*; Institution of Mechanical Engineers: London, 1996.
(12) Hansen, J. B.; Voss, B.; Joensen, F.; Siguroardottir, I. D. *SAE Tech. Pap. Ser.* **1995**, *950063*.
(13) Maricq, M. M. Szente, J. J.; Hybl, J. H. *J. Phys. Chem. A* **1997**, *101*, 5155.
(14) Japar, S. M.; Wallington, T. J.; Richert, J. F. O.; Ball, J. C. *Int. J. Chem. Kinet.* **1990**, *22*, 1257.
(15) Jenkin, M. E.; Hayman, G. D.; Wallington, T. J.; Hurley, M. D.; Ball, J. C.; Nielsen, O. J.; Ellermann, T. *J. Phys. Chem.* **1993**, *97*, 11712.
(16) Langer, S.; Ljungstrom, E.; Ellermann, T.; Nielsen, O. J.; Sehested, J. *Chem. Phys. Lett.* **1995**, *240*, 53.
(17) Sehested, J.; Sehested K.; Platz, J.; Egsgaard, H.; Nielsen, O. J. *Int. J. Chem. Kinet.* **1997**, *29*, 627.
(18) Andersen, A.; Carter, E. A. *Isr. J. Chem.* **2002**, *42*, 245.
(19) Andersen, A.; Carter, E. A. *J. Phys. Chem. A* **2003**, *107*, 9463.
(20) Pfahl, U.; Fieweger, K.; Adomeit, G. *Twenty-Sixth Symposium (International) on Combustion/The Combustion Institute*, Pittsburgh, Pennsylvania; 1996; p 781.
(21) Dagaut, P.; Boettner, J.-C.; Cathonnet, M. *Twenty-Sixth Symposium (International) on Combustion/The Combustion Institute*, Pittsburgh, Pennsylvania; 1996; p 627.
(22) Dagaut, P.; Daly, C.; Simmie, J. M.; Cathonnet, M. *Twenty-Seventh Symposium (International) on Combustion/The Combustion Institute*, Pittsburgh, Pennsylvania; 1998; p 361.
(23) Curran, H. J.; Pitz, W. J.; Westbrook, C. K.; Dagaut, P.; Boettner, J.-C.; Cathonnet, M. *Int. J. Chem. Kinet.* **1998**, *30*, 229.
(24) Fischer, S. L.; Dryer, F. L.; Curran, H. J. *Int. J. Chem. Kinet.* **2000**, *32*, 713.
(25) Curran, H. J.; Fischer, S. L.; Dryer, F. L. *Int. J. Chem. Kinet.* **2000**, *32*, 741.
(26) Liu, I.; Cant, N. W.; Bromly, J. H.; Barnes, F. J.; Nelson, P. F.; Haynes, B. S. *Chemosphere* **2001**, *42*, 583.
(27) Westley, F.; Herron, J. T.; Frizzell, D.; Hampson, R. F.; Mallard, W. G.; Mirokhin, Y,; Blakeslee, D. M. *NIST Chemical Kinetics Database*; Standard Reference Database 17-2 Q98: Gaithersburg, MD, 1998.
(28) Francisco, J. S. *J. Am. Chem. Soc.* **2003**, *125*, 10475.
(29) Kaiser, E. W. *J. Phys. Chem.* **1995**, *99*, 707.
(30) Atkinson, R.; Baulch, D. L.; Cox, R. A.; Hampson, R. F., Jr.; Kerr, J. A.; Rossi, M. J.; Troe, J. *J. Phys. Chem. Ref. Data* **1997**, *26*, 521.
(31) Lee, J. H.; Machen, R. C.; Nava, D. F.; Stief, L. J. *J. Chem. Phys.* **1981**, *74*, 2839.
(32) Batt, L.; Alvarado-Salinas, G.; Reid, I. A. B.; Robinson, C.; Smith, D. B. The Pyrolysis of Dimethyl Ether and Formaldehyde. *Nineteenth Symposium (International) on Combustion*, Pittsburgh, Pennsylvania; 1982; pp 81−87.
(33) Baulch, D. L.; Duxbury, J.; Grant, S. J.; Montague, D. C. *J. Phys. Chem. Ref. Data* **1981**, *10* (Suppl. 1), 1981.
(34) Wallington, T. J.; Hurley, M. D.; Ball, J. C. *Chem. Phys. Lett.* **1993**, *211*, 41.
(35) DeMore, W. B.; Sander, S. P.; Golden, D. M.; Hampson, R. F.; Kurylo, M. J.; Howard, C. J.; Ravishankara, A. R.; Kolb, C. E.; Molina, M. J. Chemical Kinetics and Photochemistry Data for Use in Stratospheric Modeling. Evaluation #12, *JPL Publ.* **1997**, *4*, JPL: Pasadena, California, 1997.
(36) Baulch, D. L.; Cobos, C. J.; Cox, R. A.; Esser, C.; Frank, P.; Just, Th.; Kerr, J. A.; Pilling, M. J.; Troe, J.; Walker, R. W.; Warnartz, J. *J. Phys. Chem. Ref. Data* **1992**, *21*, 411.
(37) Lightfoot, P. D.; Cox, R. A.; Crowley, J. N.; Destriau, M.; Hayman, G. D.; Jenkin, M. E.; Moortgat, G. K.; Zabel, F. *Atmos. Environ., Part A* **1992**, *26*, 1805.
(38) Zabarnick, S.; Fleming, J. W.; Lin, M. C. *Int. J. Chem. Kinet.* **1988**, *20*, 117.
(39) Baulch, D. L.; Cobos, C. J.; Cox, R. A.; Frank, P.; Hayman, G.; Just, Th.; Kerr, J. A.; Murrells, T.; Pilling, M. J.; Troe, J.; Walker, R. W. *J. Phys. Chem. Ref. Data* **1994**, *23*, 847.
(40) Veyret, B.; Rayez, J.-C.; Lesclaux, R. *J. Phys. Chem.* **1982**, *86*, 3424.
(41) Veyret, B.; Roussel, P.; Lesclaux, R. *Int. J. Chem. Kinet.* **1984**, *16*, 1599.
(42) Maricq, M. M.; Szente, J. J. *J. Phys. Chem.* **1994**, *98*, 2078.
(43) Maricq, M. M.; Szente, J. J. *J. Phys. Chem.* **1996**, *100*, 4507.
(44) Veyret, B.; Lesclaux, R.; Rayez, M.-T.; Rayez, J.-C.; Cox, R. A.; Moortgart, G. K. *J. Phys. Chem.* **1989**, *93*, 2368.